European Radiology (2023) 33:472–482
https://doi.org/10.1007/s00330-022-08982-2

UROGENITAL

Value of ^{68}Ga-labeled bombesin antagonist (RM2) in the detection of primary prostate cancer comparing with [^{18}F]fluoromethylcholine PET-CT and multiparametric MRI—a phase I/II study

Mohsen Beheshti[1,2] · Pekka Taimen[3] · Jukka Kemppainen[4] · Ivan Jambor[5,6,7] · Andre Müller[8] · Wolfgang Loidl[9] · Esa Kähkönen[10] · Meeri Käkelä[4] · Mathias Berndt[8] · Andrew W. Stephens[8] · Heikki Minn[11] · Werner Langsteger[2,12]

Received: 9 January 2022 / Revised: 12 April 2022 / Accepted: 12 June 2022 / Published online: 21 July 2022

Abstract

Objectives The bombesin derivative RM2 is a GRPr antagonist with strong binding affinity to prostate cancer (PCa). In this study, the impact of [^{68}Ga]Ga-RM2 positron emission tomography-computed tomography (PET-CT) for the detection of primary PCa was compared with that of [^{18}F]FCH PET-CT and multiparametric magnetic resonance imaging (mpMRI).

Methods This phase I/II study was conducted in 30 biopsy-positive PCa subjects. The patients were stratified into high (10 patients), intermediate (10 patients), and low risk (10 patients) for extraglandular metastases as defined by National Comprehensive Cancer Network (NCCN) criteria (NCCN Clinical Practice Guidelines in Oncology, 2016). The prostate gland was classified in 12 anatomic segments for data analysis of the imaging modalities as well as histopathologic findings. The segment with the highest radiotracer uptake was defined as the "index lesion." All cases were scheduled to undergo prostatectomy with pelvic lymph node (LN) dissection in intermediate- and high-risk patients. Intraprostatic and pelvic nodal [^{68}Ga]Ga-RM2 and [^{18}F]FCH PET-CT findings were correlated with mpMRI and histopathologic results.

Results Of the 312 analyzed regions, 120 regions (4 to 8 lesions per patient) showed abnormal findings in the prostate gland. In a region-based analysis, overall sensitivity and specificity of [^{68}Ga]Ga-RM2 PET-CT in the detection of primary tumor were 74% and 90%, respectively, while it was 60% and 80% for [^{18}F]FCH PET-CT and 72% and 89% for mpMRI. Although the overall sensitivity of [^{68}Ga]Ga-RM2 PET-CT was higher compared to that of [^{18}F]FCH PET-CT and mpMRI, the statistical analysis showed only significant difference between [^{68}Ga]Ga-RM2 PET-CT and [^{18}F]FCH PET-CT in the intermediate-risk group (p = 0.01) and [^{68}Ga]Ga-RM2 PET-CT and mpMRT in the high-risk group (p = 0.03). In the lesion-based analysis, there was no significant difference between SUVmax of [^{68}Ga]Ga-RM2 and [^{18}F]FCH PET-CT in the intraprostatic malignant lesions ([^{68}Ga]Ga-RM2: mean SUVmax: 5.98 ± 4.13, median: 4.75; [^{18}F]FCH: mean SUVmax: 6.08 ± 2.74, median: 5.5; p = 0.13).

Conclusions [^{68}Ga]Ga-RM2 showed promising PET tracer for the detection of intraprostatic PCa in a cohort of patients with different risk stratifications. However, significant differences were only found between [^{68}Ga]Ga-RM2 PET-CT and [^{18}F]FCH PET-CT in the intermediate-risk group and [^{68}Ga]Ga-RM2 PET-CT and mpMRT in the high-risk group. In addition, GRP-R-

✉ Mohsen Beheshti
m.beheshti@salk.at

1 Division of Molecular Imaging and Theranostics, Department of Nuclear Medicine & Endocrinology, University Hospital Salzburg, Paracelsus Medical University, Muellner Hauptstrasse 48, A-5020 Salzburg, Austria

2 Department of Nuclear Medicine & Endocrinology, PET-CT Center LINZ, St. Vincent's Hospital, Linz, Austria

3 Institute of Biomedicine, University of Turku, Finland and Department of Pathology, Turku University Hospital, Turku, Finland

4 Turku PET Center, Department of Nuclear Medicine, University of Turku, Turku, Finland

5 Department of Radiology, Icahn School of Medicine at Mount Sinai, New York, USA

6 Department of Radiology, University of Turku, Turku, Finland

7 Medical Imaging Centre of Southwest Finland, Turku University Hospital, Turku, Finland

8 Life Molecular Imaging GmbH, Berlin, Germany

9 Department of Urology, Ordensklinikum, Linz, Austria

10 Department of Urology, Turku University Hospital, Turku, Finland

11 Institute of Clinical Medicine, Department of Clinical Oncology, Turku University Hospital, Turku, Finland

12 Department of Nuclear Medicine, Medical University of Vienna, Vienna, Austria

based imaging seems to play a complementary role to choline-based imaging for full characterization of PCa extent and biopsy guidance in low- and intermediate-metastatic-risk PCa patients and has the potential to discriminate them from those at higher risks.

Key Points

- *[^{68}Ga]Ga-RM2 is a promising PET tracer with a high detection rate for intraprostatic PCa especially in intermediate-risk prostate cancer patients.*
- *GRPr-based imaging seems to play a complementary role to choline-based or PSMA-based PET/CT imaging in selected low- and intermediate-risk PCa patients for better characterization and eventually biopsy guidance of prostate cancer disease.*

Keywords Prostate cancer · [^{68}Ga]Ga-RM2 · [^{18}F]FCH · PET-CT · mpMRI

Abbreviations

[^{18}F]FCH	[^{18}F]fluoromethylcholine
[^{68}Ga]Ga-RM2	Gallium-68 - DOTA-4-amino-1-carboxymethylpiperidine-D-Phe-Gln-Trp-Ala-Val-Gly-His-Sta-Leu-NH2
[^{18}F]DCFPyl	2-(3-{1-Carboxy-5-[(6-[^{18}F]fluoro-pyridine-3-carbonyl)-amino]-pentyl}-ureido)-pentanedioic acid
[^{68}Ga]Ga-HBED-PSMA	^{68}Ga-Glu-NH-CO-NH-Lys(Ahx)-HBED-CC
^{11}C	Carbon-11
^{18}F	Fluorine-18
ADC	Apparent diffusion coefficient
BPH	Benign prostatic hyperplasia
CI	Confidence interval
CT	Computed tomography
DCE	Dynamic contrast enhanced
DWI	Diffuse weighted image
GRP	Gastrin-releasing-peptide receptor
LN	Lymph node
MIP	Maximum intensity projection
mpMRI	Multiparameteric prostate magnetic resonance imaging
NCCN®	National Comprehensive Cancer Network®
PCa	Prostate carcinoma
PET	Positron emission tomography
PI-RADS	Prostate Imaging–Reporting and Data System
PSA	Prostate-specific antigen
PSMA	Prostate-specific membrane antigen
RM2	DOTA-4-amino-1-carboxymethylpiperidine-D-Phe-Gln-Trp-Ala-Val-Gly-His-Sta-Leu-NH2
SPSS	Statistical Package for the Social Sciences
SUVmax	Maximum standardized uptake value
T1W	T1-weighted
T2W	T2-weighted
TRUS	Transrectal ultrasound
TSE	Turbo spin echo

Introduction

Given the multifocal nature of prostate cancer, the accurate imaging and determination of its extent make it one of the most challenging malignancies. Prostate-specific antigen (PSA) and digital rectal examination followed by transrectal ultrasound (TRUS)–guided biopsies are the standard approaches in the primary assessment of prostate cancer [1]. Due to the low diagnostic accuracy of TRUS, systematic biopsies are frequently used for the detection of prostate cancer [1]. Nevertheless, approximately one-third of cancers are missed on initial systematic biopsies [2, 3] and the Gleason score is upgraded between biopsies and radical prostatectomy [4]. Additionally, attempts to improve prostate cancer detection by intensifying the biopsy technique have not proven successful and appear to cause an increase in the risk of complications [5]. Therefore, there is an increasing need for accurate imaging modalities to guide biopsy and avoid related complications.

Multiparametric magnet resonance imaging (mpMRI) has been shown to improve diagnostic accuracy in the evaluation of intraglandular prostate cancer [6]. However, high inter-reader and inter-center variability has been reported, limiting the widespread use of mpMRI in men with diagnosed and/or suspected prostate cancer [6, 7].

Cancer diagnosis draws on the use of molecular imaging as one of its essential tools. Currently, positron emission tomography (PET) and computed tomography (CT) play a pivotal role among molecular imaging modalities, providing noninvasive information which is functional as well as anatomical. In the last decade, several PET radiotracers have been investigated through clinical trials to form an accurate depiction of intraglandular malignancies in the prostate [8–13]. PET/CT using ^{11}C- and ^{18}F-labeled choline has shown consistent reliability in diagnostic performance in the assessment of recurrent prostate cancer [9, 14]. However, its inability, in the preoperative setting, to accurately differentiate cancerous tissues from inflammatory lesions or benign prostatic hyperplasia (BPH) should be noted [10].

Gastrin-releasing peptide receptor (GRPr) proteins are highly overexpressed in multiple human tumors and have

been detected in 63–100% of human prostate cancer tissue [15, 16]. ^{68}Ga-labeled-DOTA-4-amino-1-carboxymethylpiperidine-DPhe-Gln-Trp-Ala-Val-Gly-His-Sta-Leu-NH2 ([^{68}Ga]Ga-RM2) is a synthetic bombesin receptor antagonist with high binding affinity to GRPr [17]. [^{68}Ga]Ga-RM2 PET has shown significant potential for imaging of primary prostate cancer in previous preclinical studies [18, 19]. Recently, prospective clinical trials have been conducted using [^{68}Ga]Ga-RM2 PET-CT both in staging and in recurrent prostate cancer. The primary results were promising [20, 21].

Because [^{68}Ga]Ga-RM2 and ^{18}F-choline target different biologic processes, understanding how these two tracers behave in PCa patients with different tumor characteristics and risks of metastasis is essential for determining the best management scenario.

The high diagnostic performance of PET/CT imaging using radiolabeled prostate-specific membrane antigen (PSMA) in the assessment of prostate cancer has been shown in a large number of recent published data, particularly in the recurrent setting of the disease. However, the present prospective dual-center clinical trial was designed few years ago, at a time when [^{68}Ga]Ga-PSMA was not widely available. This study was conducted to compare the diagnostic potential of PET-CT imaging for the detection of primary prostate cancer with [^{68}Ga]Ga-RM2, as a novel PET tracer, and imaging using [^{18}F]fluoromethyl-dimethyl-2-hydroxyethylammonium ([^{18}F]FCH) and to correlate the results with mpMRI. In addition, we examined the diagnostic performance of these two tracers and mpMRI in low-, intermediate-, and high-risk prostate cancer patients for intraprostatic cancer detection and extraglandular metastases. To our best knowledge, this is the earliest instance of such a study design being conducted with humans.

Materials and methods

Patients

This prospective exploratory phase I/II two-center clinical trial was performed in accordance with the principles of the 1964 Declaration of Helsinki and its later amendments or comparable standards and was approved by the ethics committees of the study centers. The study was performed in two centers (Ordensklinikum Linz, Austria, and University of Turku, Finland) and has been also registered in the European Clinical Trial Register with the register number of EudraCT-Nr.: 2014-003027-21. Signatures of the written informed consent were obtained from all subjects of the study.

The study was performed in primary staging of 30 men with biopsy-proven prostate cancer. The patients were stratified into high (10 patients), intermediate (10 patients), and low risk (10 patients) for extraglandular metastases as defined by National Comprehensive Cancer Network (NCCN) criteria [22].

The inclusion and exclusion criteria are shown in supplement 1. Radical prostatectomy was performed in all patients within a maximum interval of 4 weeks after completing the imaging modalities. In 4 patients, an old partial transurethral prostatectomy has been performed which was not pointed out by patients and was not apparent in the primary medical history of these patients. Therefore, they were excluded to avoid any bias in the results of this study. The data from 26 patients (9 low risk, 8 intermediate risk, and 9 high risk) were finally analyzed.

Safety monitoring included physical examination, electrocardiography, and laboratory parameters of various organs performed during the [^{68}Ga]Ga-RM2 PET-CT examination and 24 h as well as 3–5 days after radiotracer injection. Adverse events were documented. The common pattern of physiologic [^{68}Ga]Ga-RM2 PET biodistribution in different anatomical structures has been documented.

PET-CT imaging and data analysis

The patients underwent [^{68}Ga]Ga-RM2 PET-CT and [^{18}F]FCH PET-CT (all except 3 patients) with a maximum interval of 30 days (average: 8.7 days, range: 1–29 days). Imaging modalities have been performed at least 2 weeks after prostate biopsy.

The study was performed with dedicated PET-CT scanners (GE Healthcare, 23 patients: Discovery 710; 3 patients: Discovery VCT). Imaging was acquired 60 min after an intravenous (i.v.) injection of 4 mCi (148 MBq) of ^{68}Ga-RM2. All except 3 patients had concomitant ^{18}F-FCH PET-CT imaging 60 min after i.v. administration of 6 mCi (222 MBq) [^{18}F]FCH.

PET acquisitions were obtained from the base of the skull to the proximal of the thigh with 2.5 min/bed position acquisition time using time-of-flight (TOF) modus. All images were reconstructed identically with ordered-subsets expectation maximization algorithm (4 iterations, 18 subsets) followed by a post-reconstruction smoothing Gaussian filter (4.0 mm in full width at one-half maximum).

The CT portion of the ^{18}F-FCH PET-CT procedure was performed after intravenous infusion of 100 ml ionic contrast medium with high beam current modulation (120–330 mA, 0.6 s per rotation, 5.0 mm reconstructed section thickness, 0.5 mm overlap, 512 × 512 matrix, pitch index 1.5), while a non-contrast CT with low beam current modulation (80–120 mA) was obtained on 68Ga-RM2 PET-CT for localization and attenuation correction. The reformatted, transverse, coronal, and sagittal views were used for interpretation.

Images were read using advanced PET-CT review software (Advantage Windows, version 4.6; GE Medical Systems). More details of the PET-CT imaging are described in

supplement 2. A lesion was considered pathologic when the focal tracer accumulation was greater than the background activity. The common pattern of physiologic radiotracer distribution of 68Ga-RM2 in the study cohort has been recorded.

MRI—imaging and data analysis

Each patient was examined in the supine position in 1.5-T (n = 23) and 3-T (n = 3) scanners (Siemens, Erlangen, Germany) using surface phased-array coils or a combination of surface phased-array coils and endorectal coil.

MR data sets (T2 weighted (T2W), apparent diffusion coefficient (ADC), and dynamic contrast enhanced (DCE)) were evaluated qualitatively based on the PI-RADS (version 2.1) scoring system for the tumor detection and localization. mpMRI images have been reported by experienced radiologists in each study center in the setting of daily work routine. In addition, central (external) reading was performed by an experienced radiologist (> 10 years). Further details of prostate MRI protocol are presented in supplement 2.

Data reading and final interpretation

A systematic approach of double reading was performed for all imaging and histopathologic data (Fig. 1). The prostate gland was classified into 12 anatomic segments for data analysis of both imaging and histopathologic findings. The segment with the highest radiotracer uptake was defined as the "index lesion" on PET/CT.

mpMRI images were read both in the setting of clinical routine as well as central external reading by experienced radiologists (> 10 years).

The final diagnosis of imaging results was based on histopathological findings as "gold standard." All data and the discrepancies between readers have been discussed in a consensus meeting, in that all experts from different disciplines participated. The final interpretation of the imaging findings was made by reviewing the histopathological results and a consensus between readers.

Statistical analysis

Univariate analysis was performed to assess the variables and frequency tables. Quantitative variables were summarized using descriptive statistics (mean ± SD) and were compared in different groups using the independent t test. The paired t test was used to compare quantitative variables in a paired group. Sensitivity and specificity were calculated using data collected from PET studies on a per-region basis. Clopper-Pearson's correlation coefficient was calculated for correlations between different quantitative variables. Statistical analysis was conducted using SPSS software version 24 (SPSS

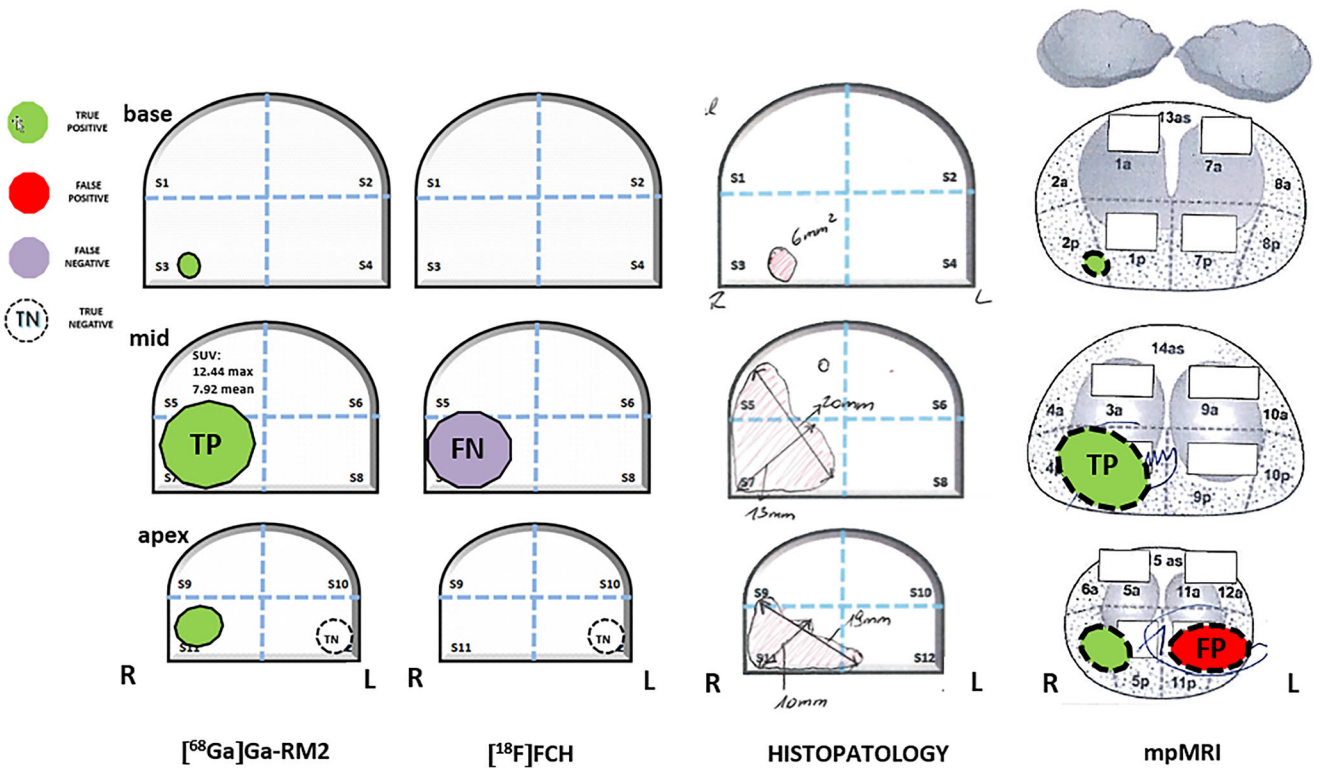

Fig. 1 Schematic presentation of the methodological approach for segmentation of the prostate gland and systematic reading of imaging modalities and correlation with histopathological findings. It refers to the data presented on Fig. 2

Inc.). A value of $p < 0.05$ was considered to indicate statistical significance in all comparisons.

Results

Biodistribution and safety

No adverse clinical reactions, abnormal laboratory findings, or side effects were detected during the 3–5 days after intravenous administration of [^{68}Ga]Ga-RM2.

High physiological [^{68}Ga]Ga-RM2 uptake was recorded in the pancreas and, because of its renal excretion, in the urinary tract. Mildly to moderately increased uptake was observed in the gastrointestinal tract. The liver, spleen, and bone marrow showed no noticeable physiological uptake (Figs. 2, 3, 4, and 5A).

Primary tumor

[^{68}Ga]Ga-RM2 PET-CT was able to detect at least 1 index lesion in the prostate gland of 83% (20/24) of patients with positive results in the final histopathology, while [^{18}F]FCH PET-CT and mpMRI detected at least 1 index lesion in 76% (16/21) and 96% (23/24) of patients, respectively (Fig. 2).

In 2 low-risk patients with initially positive biopsy reports, final histopathology showed only 2- and 5-mm microfoci of Gleason 3 + 3 carcinoma but no clinical significance for the final correlation analyses with imaging findings.

Region-based analysis

Of the overall 312 analyzed regions, 120 regions (4 to 8 lesions per patient) showed abnormal findings in the prostate gland either on imaging modalities and/or on histopathology. Histopathological findings confirmed cancerous tissue in 50 (42%) regions, while 70 regions showed no evidence of tumor infiltration (Table 1). Overall, sensitivity and specificity of [^{68}Ga]Ga-RM2 PET-CT, [^{18}F]FCH PET-CT, and mpMRI in the detection of primary tumor were 74% [95% confidence interval (95% CI): 62–86] and 90% (95% CI: 83–97), 60% (95% CI: 46–74) and 80% (95% CI: 70–90), and 72% (95% CI: 60–84) and 89% (95% CI: 81–96), respectively. The sensitivity and specificity of each imaging modality in low-, intermediate-, and high-risk patients are presented in Table 1. Although the overall sensitivity of [^{68}Ga]Ga-RM2 PET-CT

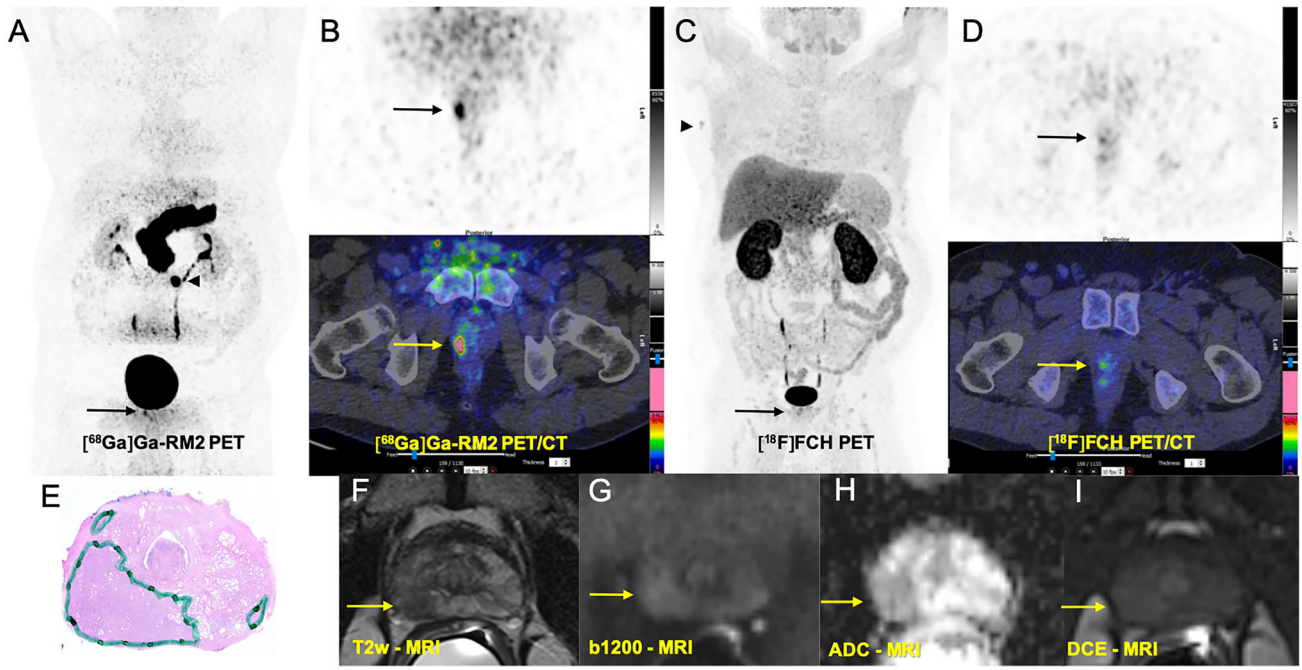

Fig. 2 Comparison of [68Ga]Ga-RM2 PET-CT with [18F]FCH PET-CT and mpMRI in pre-operative staging of a prostate cancer patient with intermediate risk of extraglandular metastases (PSA: 9.0 ng/ml, Gleason score: 7 (4 + 3), grade 3, TNM: pT2c N0 (0/14) R0 L0 V0 Pn1). **A** [^{68}Ga]Ga-RM2 PET: maximum intensity projection (MIP) shows intensive physiologic tracer uptake in the pancreas with a focal non-specific bowel uptake on the middle of the left abdomen (arrowhead). A focal tracer uptake is evident in the right prostate lobe (arrow). **B** Axial view [^{68}Ga]Ga-RM2 PET-CT (PET: upper, fusion PET-CT: middle) from the prostate region showing intensive focal uptake on the left prostate lobe (arrows) corresponding with the findings on histopathology (malignancy is marked) (**E**). [^{18}F]FCH PET-CT MIP (**C**) axial view of the prostate region (**D**): mild focal uptake is seen on the right axillary region, suggestive of reactive lymph node. No appreciable [^{18}F]FCH uptake is seen on the prostate. T2-weighted image (**F**) demonstrated a focal area of decreased signal in the left peripheral zone (yellow arrow) with corresponding diffusion-weighted imaging signal restriction (trace *b* values of 1200 s/mm^2, **G**; ADC, **H**) and early contrast enhancement (dynamic contrast enhancement, DCE, **I**). Overall, these findings represented a PI-RADs version 2.1 score 5 lesion

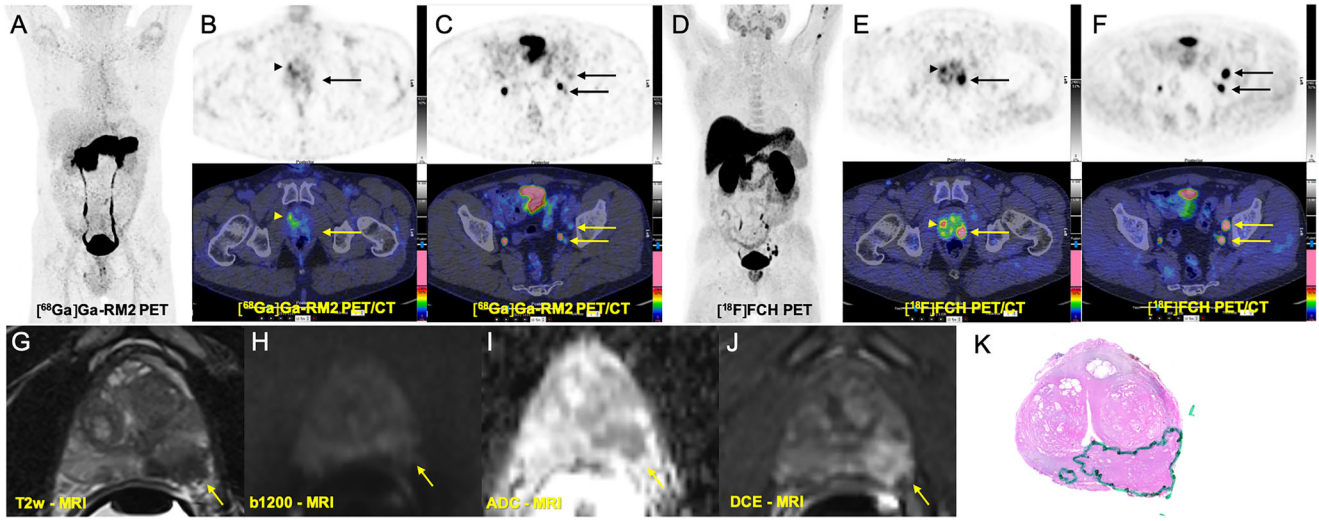

Fig. 3 Comparison of [^{68}Ga]Ga-RM2 PET-CT with [^{18}F]FCH PET-CT and mpMRI in pre-operative staging of a prostate cancer patient with high risk of extraglandular metastases (PSA: 30.0 ng/ml, Gleason score: 8 (4 + 4), grade 3, TNM: pT3b pN1 (3/14) R1 (Apex li) L0 V0 Pn1). **A** [^{68}Ga]Ga-RM2 PET: maximum intensity projection (MIP) shows mild focal tracer uptake on the right prostate lobe (arrowhead). **B** Axial view [^{68}Ga]Ga-RM2 PET-CT (PET: upper, fusion PET-CT: lower row) from the prostate region shows mild focal tracer uptake on the right prostate lobe (arrowhead) without corresponding malignant findings on histopathology (false positive). **C** Axial view [^{68}Ga]Ga-RM2 PET-CT (PET: upper, fusion PET-CT: lower row) from the pelvis shows only faint tracer uptakes on the lymph nodes on the left iliac region (arrows). **D** [^{18}F]FCH PET-CT MIP. **E** Axial view [^{18}F]FCH PET-CT (PET: upper, fusion PET-CT: middle) from the prostate region shows intensive focal tracer uptake on the left prostate lobe (arrows) corresponding with malignant findings on histopathology **(K)** (true positive). A focal tracer uptake is also seen on the right prostate lobe (arrowhead) without corresponding malignant findings on histopathology (false positive). **F** Axial view [^{18}F]FCH PET-CT from the pelvis shows intensive focal tracer uptakes on the lymph nodes on the left iliac region (arrows), verified as metastases on histhopathology (true positive). T2-weighted image (**G**) demonstrated a focal area of decreased signal in the right peripheral zone (yellow arrow) with corresponding diffusion-weighted imaging signal restriction (trace *b* values of 1200 s/mm^2, **H**; ADC, **I**) and early contrast enhancement (dynamic contrast enhancement, DCE, **J**). Overall, these findings represented a PI-RADs version 2.1 score 5 lesion

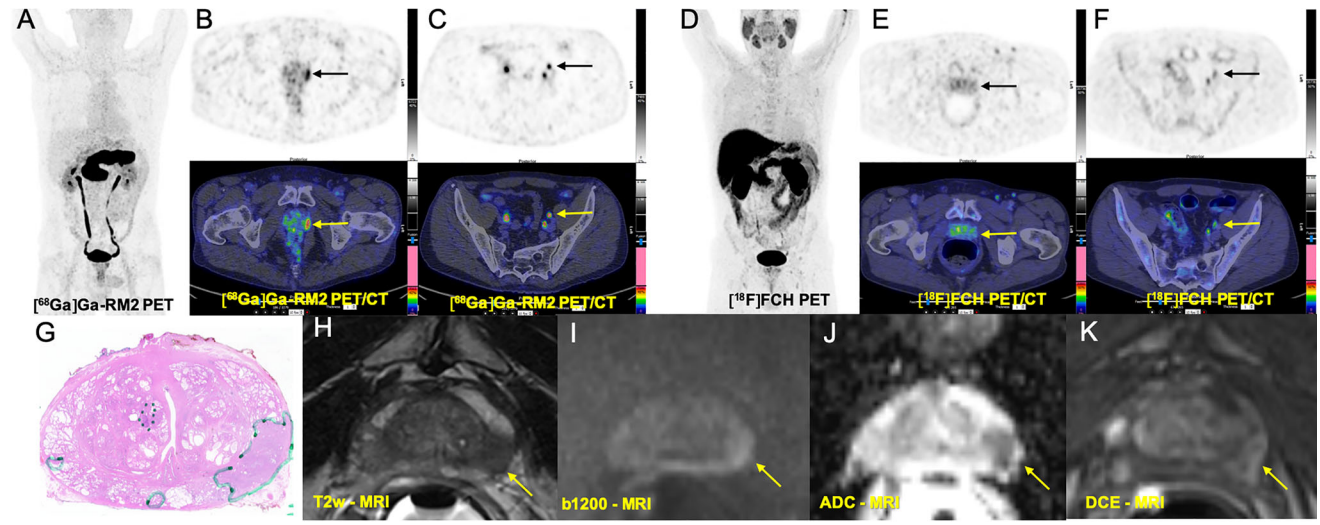

Fig. 4 Comparison of [^{68}Ga]Ga-RM2 PET-CT with [^{18}F]FCH PET-CT and mpMRI in pre-operative staging of a prostate cancer patient with high risk of extraglandular metastases (PSA: 4.49 ng/ml, Gleason score: 9 (4 + 5), pT3a N1 (1/23) R0 L1 V0 Pn1). **A** [^{68}Ga]Ga-RM2 PET: maximum intensity projection. **B** Axial view [^{68}Ga]Ga-RM2 PET-CT (PET: upper, fusion PET-CT: lower) from the prostate region shows moderate focal tracer uptake on the left prostate lobe (arrows) corresponding to malignant finding on histopathology (**G**) (true positive). **C** Axial view [^{68}Ga]Ga-RM2 PET-CT (PET: upper, fusion PET-CT: lower row) from the pelvis shows focal tracer uptake on a lymph node on the left iliac region (arrows). **D** [^{18}F]FCH PET-CT MIP. **E** Axial view [^{18}F]FCH PET-CT (PET: upper, fusion PET-CT: lower row) from the prostate region shows no remarkable tracer uptake on the prostate (arrows) (false negative). **F** Axial view [^{18}F]FCH PET-CT from the pelvis shows only faint focal tracer uptake on the lymph node on the left iliac region (arrows). T2-weighted image (**H**) demonstrats a focal area of decreased signal in the left peripheral zone (yellow arrow) with corresponding diffusion-weighted imaging signal restriction (trace *b* values of 1200 s/mm^2, **I**; ADC, **J**) and early contrast enhancement (dynamic contrast enhancement, DCE, **K**). Overall, these findings represent a PI-RADs version 2.1 score 5 lesion

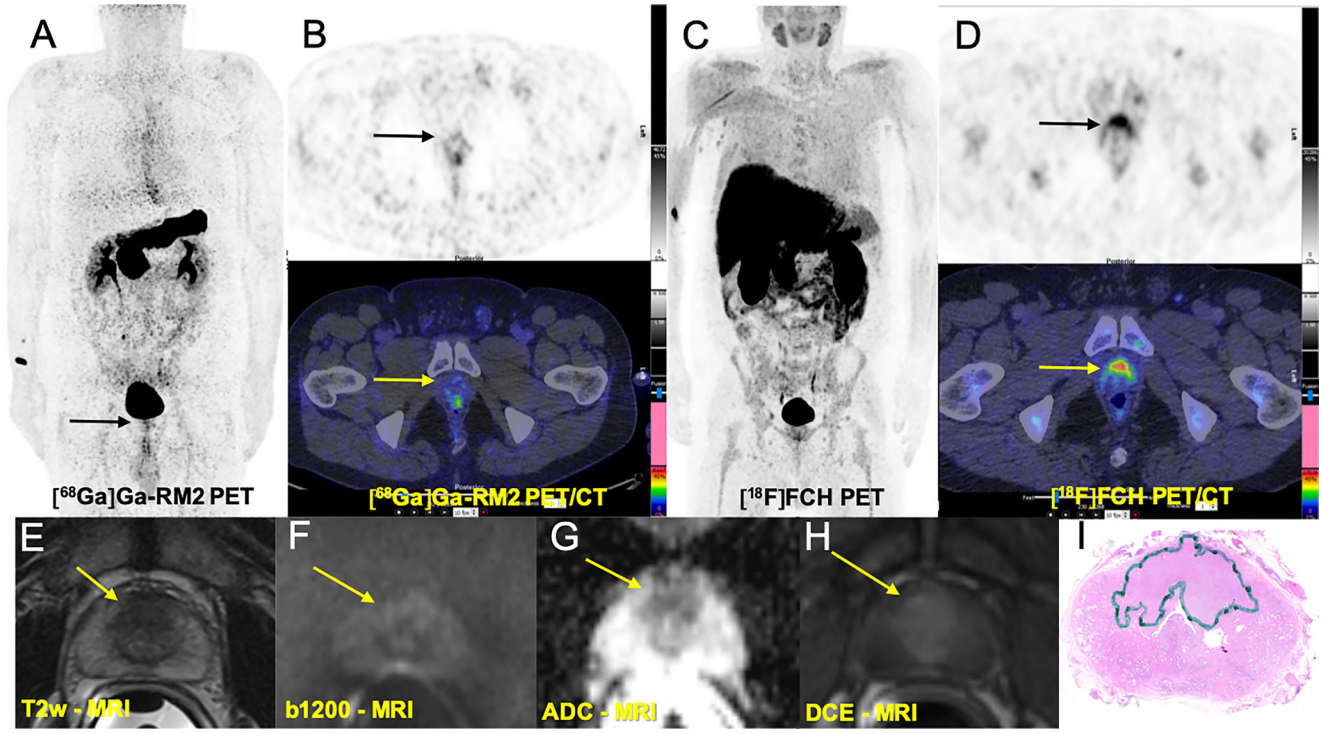

Fig. 5 Comparison of [^{68}Ga]Ga-RM2 PET-CT with [^{18}F]FCH PET-CT and mpMRI in pre-operative staging of a prostate cancer patient with high risk of extraglandular metastases (PSA: 21.6 ng/ml, Gleason score: 7 (4 + 3), pT3a pN0 pR1 L0 V0 pn1. **A** [^{68}Ga]Ga-RM2 PET: maximum intensity projection. **B** Axial view [^{68}Ga]Ga-RM2 PET-CT (PET: upper, fusion PET-CT: lower row) from the prostate region shows no remarkable tracer uptake on the (arrows) (false negative). **D** [^{18}F]FCH PET-CT MIP. **E** Axial view [^{18}F]FCH PET-CT (PET: upper, fusion PET-CT: lower row) from the prostate region shows intensive tracer uptake at the apical anterior part of the prostate (arrows) corresponding to malignant finding on histopathology (**I**) (true positive). T2-weighted image (**E**) demonstrated a focal area of decreased signal in the central gland, anterior to the urethra (yellow arrow) with corresponding diffusion-weighted imaging signal restriction (trace *b* values of 1200 s/mm^2, **F**; ADC, **G**) and early contrast enhancement (dynamic contrast enhancement, DCE, **H**). Overall, these findings represented a PI-RADs version 2.1 score 5 lesion

Table 1 Details of positive and negative histopathological findings in the region-based analysis and sensitivity and specificity of each imaging modality in low-, intermediate-, and high-risk patients

Region	Number/Percentage	Positive	Negative
Overall	**120**	**50 (42%)**	**70 (58%)**
Low risk	36	13 (36%)	23 (64%)
Intermediate risk	40	20 (50%)	20 (50%)
High risk	44	17 (39%)	27 (61%)
Sensitivity	**[^{68}Ga]Ga-RM2**	**[^{18}F]FCH**	**mpMRI**
Overall	**74%**	**60%**	**72%**
Low risk	77%	69%	69%
Intermediate risk	80%	42%	55%
High risk	65%	73%	94%
Specificity	**[^{68}Ga]Ga-RM2**	**[^{18}F]FCH**	**mpMRI**
Overall	**90%**	**80%**	**89%**
Low risk	83%	61%	87%
Intermediate risk	90%	94%	85%
High risk	96%	90%	93%

was higher compared to that of [^{18}F]FCH PET-CT and mpMRI, the statistical analysis showed only significant difference between [^{68}Ga]Ga-RM2 PET-CT and [^{18}F]FCH PET-CT in the intermediate-risk group (p = 0.01) and [^{68}Ga]Ga-RM2 PET-CT and mpMRT in the high-risk group (p = 0.03).

Lesion-based analysis

Overall, 56 lesions were analyzed in prostate glands on [^{68}Ga]Ga-RM2 PET-CT and mpMRI and 51 lesions on [^{18}F]FCH PET-CT. The difference between analyzed lesions was due to lack of performance of [^{18}F]FCH PET-CT in 3 patients. Histopathological results showed prostate cancer in 39 lesions. The sensitivity of [^{68}Ga]Ga-RM2 PET-CT, [^{18}F]FCH PET-CT, and mpMRI in the detection of primary tumor was 74% (95% CI 61–88), 61% (95% CI 45–77), and 67% (95% CI 52–82), respectively. The sensitivity and positive predictive value of each imaging modality in low-, intermediate-, and high-risk patients are displayed in Table 2.

Overall, there was no significant difference between the SUVmax of [^{68}Ga]Ga-RM2 and [^{18}F]FCH PET-CT in the

Table 2 Lesion-based analysis: sensitivity, mean of maximum standardized uptake value (mean SUVmax), and positive predictive value (PPV) of each imaging modality in low-, intermediate-, and high-risk patients

Sensitivity	[^{68}Ga]Ga-RM2 (mean SUVmax, *p* value)	[^{18}F]FCH (mean SUVmax)	mpMRI
Overall	**74% (5.98 ± 4.13; *p* = 0–13)**	**61% (6.08 ± 2.74)**	**67%**
Low risk	77% (6.78 ± 5.07; *p* = 0.68)	62% (6.05 ± 2.11)	62%
Intermediate risk	80% (6.16 ± 3.67; *p* = 0.13)	50% (5.16 ± 1.63)	53%
High risk	64% (4.66 ± 2.60; *p* = 0.19)	78% (6.45 ± 3.30)	91%
PPV	**[^{68}Ga]Ga-RM2**	**[^{18}F]FCH**	**mpMRI**
Overall	**81%**	**67%**	**79%**
Low risk	71%	50%	80%
Intermediate risk	80%	50%	53%
High risk	64%	78%	91%

intraprostatic malignant lesions ([^{68}Ga]Ga-RM2: mean SUVmax 5.98 ± 4.13, median: 4.75; [^{18}F]FCH: mean SUVmax 6.08 ± 2.74; median: 5.5; p = 0.13). However, the mean SUVmax of index lesions was significantly higher on [^{68}Ga]Ga-RM2 compared to that of [^{18}F]FCH PET-CT ([^{68}Ga]Ga-RM2: mean SUVmax 7.89 ± 4.94; [^{18}F]FCH: mean SUVmax 5.34 ± 2.52; p = 0.03). A differentiation between malignant and BPH was not possible using an SUV-cutoff neither on [^{68}Ga]Ga-RM2 nor on [^{18}F]FCH PET-CT. However, the tumor to background ratio was 2.5 on ^{68}Ga-RM2 PET-CT compared to 2.0 on [^{18}F]FCH PET-CT (p = 0.21). Although the mean SUVmax was higher in the low-risk and intermediate-risk compared to that in the high-risk patients on [^{68}Ga]Ga-RM2 PET-CT, the difference was not statistically significant and we did not find any SUV cutoff in order to predict the risk classification (Table 2). Also, there was no significant difference between mean SUVmax of various risk groups on [^{18}F]FCH PET-CT (Table 2).

Lymph node and distant metastases

Lymph node metastases were detected in 2 patients. In 1 high-risk patient with a PSA value of 30 ng/ml and Gleason score of 8 (4 + 4) with 4 regional lymph node metastases, [^{18}F]FCH PET-CT was able to detect 1 additional lymph node (diameter 15 mm) in the internal iliac region, which was negative on [^{68}Ga]Ga-RM2 PET-CT. Overall, the detected lymph nodes on [^{18}F]FCH PET-CT showed markedly higher uptake (mean SUVmax: 13.5 ± 3.72) compared to those detected on [^{68}Ga]Ga-RM2 PET-CT (mean SUVmax: 3.92 ± 0.70) (Fig. 3). In contrast, in another high-risk patient with a PSA value of 4.9 ng/ml and Gleason score of 9 (4 + 5), [^{68}Ga]Ga-RM2 PET-CT detected 1 metastatic regional lymph node with a diameter of 9 mm in the external iliac region (SUVmax: 6.9), which was negative on [^{18}F]FCH PET-CT. No distant metastases were detected in our patient population (Fig. 4).

Discussion

There are currently tremendous efforts on developing novel PET radiotracers, which can accurately detect intraprostatic cancer and differentiate malignant from BPH and inflammatory lesions.

The aim of the present study was to investigate the diagnostic accuracy of [^{68}Ga]Ga-RM2 PET-CT compared to that of ^{18}F-FCH PET-CT and mpMRI in the detection of primary prostate cancer. Furthermore, the pattern of tracer uptake on PET-CT was correlated with tumor characteristics on histopathology in low-, intermediate-, and high-risk PCa patients.

In a region-based analysis, the sensitivity and specificity of [^{68}Ga]Ga-RM2 PET-CT were superior to those of ^{18}F-FCH PET-CT and comparable to those of mpMRI. In overall assessment, there was no significant difference in the diagnostic accuracy of the different modalities. However, [^{68}Ga]Ga-RM2 PET-CT showed significantly higher sensitivity compared to [^{18}F]FCH PET-CT in intermediate-risk prostate cancer patients and mpMRI revealed significantly higher sensitivity in high-risk cases. In the lesion-based analysis, overall, 39 PCa lesions were defined in histopathology. [^{68}Ga]Ga-RM2 PET-CT showed superior sensitivity of 74% in the detection of primary tumor compared to [^{18}F]FCH PET-CT and mpMRI with a sensitivity of 61% and 67%, respectively. The overall findings of the present investigation are in concordance with those of similar studies [10, 18, 20, 23, 24]. To our best knowledge, this is the first prospective clinical investigation that explicitly evaluates the impact of [^{68}Ga]Ga-RM2 PET-CT and compare its value with that of [^{18}F]FCH PET-CT in three patients' cohorts with different metastatic risk stratifications, in which all patients underwent radical prostatectomy. When correlating the diagnostic accuracy of [^{68}Ga]Ga-RM2 PET-CT with biological tumor characteristics and metastatic risks, we noticed, both on region- and lesion-based analyses, limited sensitivity of 65% in the high-risk patient's group compared to 74% for [^{18}F]FCH PET-CT and 94% for mpMRI (Fig. 5). In contrast, the [^{68}Ga]Ga-RM2 PET-CT showed significantly higher sensitivity of 80% in

intermediate-risk cases compared to 42% and 55% for [^{18}F]FCH PET-CT and mpMRI, respectively. These findings are not in line with the data presented by Kähkönen et al, who reported markedly higher sensitivity of [^{68}Ga]Ga-RM2 PET-CT of 88% for the detection of primary tumor in 11 high-risk PCa patients [18]. This different sensitivity might be explained by the more advanced tumor stage in that study, as higher T-categories were reported in their patients compared to our high-risk cohort [23]. Nevertheless, an accurate conclusion cannot be drawn because of the low number of the patients in both studies.

In the last years, tremendous investigations have been done for developing radioligands targeting prostate-specific-membrane antigen (PSMA) for the depiction of malignant tissues particularly in prostate cancer and several small-molecule tracers targeting PSMA have generated a lot of interest [25–27].

[^{68}Ga]Ga-PSMA and [^{18}F]PSMA tracers in conjunction with both PET-CT and PET/MRI have emerged as promising imaging modalities for primary staging and restaging of PCa [28–31]. However, there are still limited prospective data on the impact of ^{68}Ga-labeled PSMA PET-CT for intraglandular detection of PCa [32]. A subanalysis of prospective data of [^{68}Ga]Ga-PSMA PET/MRI in PCa showed significant differences in tracer uptake of the dominant intraprostatic cancer tissue between postoperative low/intermediate-risk patients and high-risk subjects [31]. In a recent preclinical study, the authors retrospectively compared the binding of radiolabeled GRPr-antagonists (i.e., [^{111}In]RM2) with [^{111}In]PSMA-617 in 20 frozen prostatectomy samples with various metastatic risks of the D'Amico classification [33]. They reported a significantly higher binding affinity of [^{111}In]RM2 in low-metastatic-risk samples with low Gleason score and low PSA value, while the binding of [^{111}In]PSMA-617 was high in almost all cancerous tissues independent of metastatic risk, Gleason score, or PSA value. The authors concluded that GRPr and PSMA-based imaging may have a complimentary role to fully characterize prostate cancer disease, GRPr being targeted in low-metastatic-risk patients while PSMA could be a valuable target in higher risks.

The findings of the current study support the data from previous investigations showing that [^{68}Ga]Ga-RM2 PET-CT detected more intraglandular prostate cancer lesions in the low-risk group. However, we found no correlation between tracer uptake by means of SUVmax on [^{68}Ga]Ga-RM2 and [^{18}F]FCH PET-CT and Gleason score, PSA value, and risk of metastases, in line with previous clinical reports [20, 23]. There was also no relevant trend in the increasing pattern of SUVmax relating to PSA value and/or Gleason score. Although the results of latter preclinical investigation agree with the known increased GRPr expression in low-grade prostate cancer, in vitro and preclinical results may not necessarily represent the imaging findings on humans.

In one of the early studies evaluating the impact of ^{68}Ga-labeled Bombesin antagonists in prostate cancer, the authors observed a significant difference in SUV between cancerous and hyperplastic prostatic lesions [18]. Although less false-positive intraprostatic lesions were seen on [^{68}Ga]Ga-RM2 PET compared to [^{18}F]FCH PET (i.e., 7 versus 11, respectively), a differentiation between malignant and BPH was not possible using a SUV-cutoff neither by [^{68}Ga]Ga-RM2 nor [^{18}F]FCH PET-CT. The different findings may be related to the selection bias, as most of the patients undergoing surgery in that study belonged to the high-clinical-risk group with high risk of lymph node metastasis.

Touijer et al recently published clinical data in 16 patients with biopsy-proven primary PCa with low (n = 2), intermediate (n = 8), and high risk (n = 6) of recurrence. The sensitivity, specificity, and accuracy of 85.2%, 81.3%, and 83.9% were reported for fused [^{68}Ga]Ga-RM2 PET-CT-mpMRI. The average SUVmax ranged from 1.5 to 27.8 (mean: 9.1) for dominant tumors and 0.45 to 7.1 (mean: 3.7) for BPH. However, no correlation was found between SUVmax and Gleason score [20]. The higher diagnostic performance can be explained by using both [^{68}Ga]Ga-RM2 PET-CT and mpMRI findings and the higher number of patients with intermediate risk.

Despite the intention of gaining information on extraprostatic metastases in the high-risk group, only two cases out of the 10 showed metastases, so limited conclusions can be made. In the detection of lymph node metastases, [^{68}Ga]Ga-RM2 and [^{18}F]FCH PET-CT showed contradicting findings in two high-risk PCa patients (Figs. 3 and 4). This may be related to the PSA value of these patients; however, because of the limited number of patients with lymph node metastases, the impact of [^{68}Ga]Ga-RM2 PET-CT in the assessment of lymph node metastases remains inconclusive.

Our findings in this study may have future clinical impact. Prostate cancer patients with low metastatic risk are today not eligible for radical treatments anymore but rather to active surveillance or local treatments [34]. In addition, Gleason score is upgraded in about 30% of PCa patients between biopsies and radical prostatectomy [35]. Thus, an imaging procedure capable to discriminate "true" low and intermediate from high metastatic risks would be helpful to schedule local treatments in this group of patients. Results of this work indicate that GRPr targeting by hybrid imaging (e.g. PET/MRI) seems promising procedure amenable to better biopsy guidance in low- and intermediate-metastatic-risk PCa patients and has the potential to discriminate them from PCa patients with higher risks. In addition, GRPr-based imaging seems to play a complementary role to PSMA-based or Choline-based imaging for fully characterization of prostate cancer disease.

The main limitation of this study was the small number of patients in each risk group, mainly due to the exploratory design of this research. Thus, given the exploratory nature of this phase I/II study and the relatively small sample size, *p*-values without correction for multiple comparisons were reported as guidance, but they should not be interpreted as a formal hypotheses testing. In addition, [^{18}F]FCH appears to be outperformed by PSMA-radiotracers in light of evolving data showing the value of PSMA-based PET-CT in PCa. This could moderate the clinical impact of this study.

Conclusion

[^{68}Ga]Ga-RM2 is a promising new PET tracer with a high detection rate for intraprostatic PCa. In addition, GRPr-based imaging can play a complementary role to choline-based or PSMA-based imaging for full characterization of prostate cancer disease and biopsy guidance in low- and intermediate-metastatic-risk PCa patients and has the potential to discriminate them from those of higher risks.

Supplementary Information The online version contains supplementary material available at https://doi.org/10.1007/s00330-022-08982-2.

Acknowledgements The abstract of the results of this study has been presented in the "Clinical Oncology: Prostate" session (OP348) of the annual congress of the European Society of Nuclear Medicine 2016 (EANM'16).

There is pre-print publication of this study that can be found at //www.researchsquare.com/article/rs-809326/v1.

Funding Open access funding provided by Paracelsus Medical University. This study has received funding from Life Molecular Imaging GmbH (previous Piramal Imaging GmbH), Berlin, Germany.

Declarations

Guarantor The scientific guarantor of this study is Mohsen Beheshti MD, FEBNM, FASNC, professor and head of the Division of Molecular Imaging and Theranostics, Department of Nuclear Medicine & Endocrinology, University Hospital Salzburg, Paracelsus Medical University, Salzburg, Austria

Conflict of interest Andre Müller, Mathias Berndt, and Andrew W. Stephens are employees of Life Molecular Imaging GmbH (previous Piramal Imaging GmbH), Berlin, Germany. The other authors declare no relationships with any companies, whose products or services may be related to the subject matter of the article.

Statistics and biometry One of the authors has significant statistical expertise.

Informed consent Written informed consent was obtained from all subjects (patients) this study.

Ethical approval Institutional Review Board approval was obtained. The study has been also registered in the European Clinical Trial Register with the register number of EudraCT-Nr.: 2014-003027-21.

Methodology

- Prospective
- Diagnostic or prognostic study
- Multicenter study

References

1. Halpern EJ, Frauscher F, Strup SE, Nazarian LN, O'Kane P, Gomella LG (2002) Prostate: high-frequency Doppler US imaging for cancer detection. Radiology 225:71–77
2. Djavan B, Ravery V, Zlotta A et al (2001) Prospective evaluation of prostate cancer detected on biopsies 1, 2, 3 and 4: when should we stop? J Urol 166:1679–1683
3. Roehl KA, Antenor JA, Catalona WJ (2002) Serial biopsy results in prostate cancer screening study. J Urol 167:2435–2439
4. Rajinikanth A, Manoharan M, Soloway CT, Civantos FJ, Soloway MS (2008) Trends in Gleason score: concordance between biopsy and prostatectomy over 15 years. Urology 72:177–182
5. Simon J, Kuefer R, Bartsch G Jr, Volkmer BG, Hautmann RE, Gottfried HW (2008) Intensifying the saturation biopsy technique for detecting prostate cancer after previous negative biopsies: a step in the wrong direction. BJU Int 102:459–462
6. Hoeks CM, Barentsz JO, Hambrock T et al (2011) Prostate cancer: multiparametric MR imaging for detection, localization, and staging. Radiology 261:46–66
7. Hricak H, Choyke PL, Eberhardt SC, Leibel SA, Scardino PT (2007) Imaging prostate cancer: a multidisciplinary perspective. Radiology 243:28–53
8. Jadvar H (2009) Molecular imaging of prostate cancer with 18F-fluorodeoxyglucose PET. Nat Rev Urol 6:317–323
9. Beheshti M, Haim S, Zakavi R et al Impact of 18F-choline PET/CT in prostate cancer patients with biochemical recurrence: influence of androgen deprivation therapy and correlation with PSA kinetics. J Nucl Med 54:833-840
10. Vali R, Loidl W, Pirich C, Langesteger W, Beheshti M (2015) Imaging of prostate cancer with PET/CT using (18)F-Fluorocholine. Am J Nucl Med Mol Imaging 5:96–108
11. Dehdashti F, Picus J, Michalski JM et al (2005) Positron tomographic assessment of androgen receptors in prostatic carcinoma. Eur J Nucl Med Mol Imaging 32:344–350
12. Kato T, Tsukamoto E, Kuge Y et al (2002) Accumulation of [11C]acetate in normal prostate and benign prostatic hyperplasia: comparison with prostate cancer. Eur J Nucl Med Mol Imaging 29:1492–1495
13. Schuster DM, Savir-Baruch B, Nieh PT et al Detection of recurrent prostate carcinoma with anti-1-amino-3-18F-fluorocyclobutane-1-carboxylic acid PET/CT and 111In-capromab pendetide SPECT/CT. Radiology 259:852-861

14. Beheshti M, Langsteger W, Fogelman I (2009) Prostate cancer: role of SPECT and PET in imaging bone metastases. Semin Nucl Med 39:396–407
15. Reubi JC, Wenger S, Schmuckli-Maurer J, Schaer JC, Gugger M (2002) Bombesin receptor subtypes in human cancers: detection with the universal radioligand (125)I-[D-TYR(6), beta-ALA(11), PHE(13), NLE(14)] bombesin(6-14). Clin Cancer Res 8:1139–1146
16. Sun B, Halmos G, Schally AV, Wang X, Martinez M (2000) Presence of receptors for bombesin/gastrin-releasing peptide and mRNA for three receptor subtypes in human prostate cancers. Prostate 42:295–303
17. Jensen RT, Battey JF, Spindel ER, Benya RV (2008) International Union of Pharmacology. LXVIII. Mammalian bombesin receptors: nomenclature, distribution, pharmacology, signaling, and functions in normal and disease states. Pharmacol Rev 60:1–42
18. Kahkonen E, Jambor I, Kemppainen J et al (2013) In vivo imaging of prostate cancer using [68Ga]-labeled bombesin analog BAY86-7548. Clin Cancer Res 19:5434–5443
19. Zhang H, Desai P, Koike Y et al (2017) Dual-modality imaging of prostate cancer with a fluorescent and radiogallium-labeled gastrin-releasing peptide receptor antagonist. J Nucl Med 58:29–35
20. Touijer KA, Michaud L, Alvarez HAV et al (2019) Prospective study of the radiolabeled GRPR antagonist BAY86-7548 for positron emission tomography/computed tomography imaging of newly diagnosed prostate cancer. Eur Urol Oncol 2:166–173
21. Minamimoto R, Sonni I, Hancock S et al (2018) Prospective evaluation of (68)Ga-RM2 PET/MRI in patients with biochemical recurrence of prostate cancer and negative findings on conventional imaging. J Nucl Med 59:803–808
22. NCCN clinical practice guidelines in oncology. Prostate Cancer Available via www.NCCN.orgVersion 3.2016
23. Fassbender TF, Schiller F, Mix M et al (2019) Accuracy of [(68)Ga]Ga-RM2-PET/CT for diagnosis of primary prostate cancer compared to histopathology. Nucl Med Biol 70:32–38
24. Husarik DB, Miralbell R, Dubs M et al (2008) Evaluation of [(18)F]-choline PET/CT for staging and restaging of prostate cancer. Eur J Nucl Med Mol Imaging 35:253–263
25. Perera M, Papa N, Christidis D et al (2016) Sensitivity, Specificity, and Predictors of Positive (68)Ga-Prostate-specific membrane antigen positron emission tomography in advanced prostate cancer: a systematic review and meta-analysis. Eur Urol 70:926–937
26. Cuccurullo V, Di Stasio GD, Mansi L (2018) Nuclear medicine in prostate cancer: a new era for radiotracers. World J Nucl Med 17:70–78
27. Lutje S, Heskamp S, Cornelissen AS et al (2015) PSMA ligands for radionuclide imaging and therapy of prostate cancer: clinical status. Theranostics 5:1388–1401
28. Budaus L, Leyh-Bannurah SR, Salomon G et al (2016) Initial experience of (68)Ga-PSMA PET/CT Imaging in high-risk prostate cancer patients prior to radical prostatectomy. Eur Urol 69:393–396
29. Eiber M, Weirich G, Holzapfel K et al (2016) Simultaneous (68)Ga-PSMA HBED-CC PET/MRI improves the localization of primary prostate cancer. Eur Urol 70:829–836
30. Fendler WP, Schmidt DF, Wenter V et al (2016) 68Ga-PSMA PET/CT detects the Location and Extent of Primary Prostate Cancer. J Nucl Med 57:1720–1725
31. Grubmuller B, Baltzer P, Hartenbach S et al (2018) PSMA Ligand PET/MRI for Primary Prostate Cancer: Staging Performance and Clinical Impact. Clin Cancer Res 24:6300–6307
32. Hofman MS, Lawrentschuk N, Francis RJ et al (2020) Prostate-specific membrane antigen PET-CT in patients with high-risk prostate cancer before curative-intent surgery or radiotherapy (proPSMA): a prospective, randomised, multicentre study. Lancet 395:1208–1216
33. Schollhammer R, De Clermont GH, Yacoub M et al (2019) Comparison of the radiolabeled PSMA-inhibitor (111)In-PSMA-617 and the radiolabeled GRP-R antagonist (111)In-RM2 in primary prostate cancer samples. EJNMMI Res 9:52
34. Moschini M, Carroll PR, Eggener SE et al (2017) Low-risk prostate cancer: identification, management, and outcomes. Eur Urol 72:238–249
35. Porcaro AB, Siracusano S, de Luyk N et al (2017) Low-risk prostate cancer and tumor upgrading in the surgical specimen: analysis of clinical factors predicting tumor upgrading in a contemporary series of patients who were evaluated according to the modified Gleason Score grading system. Curr Urol 10:118–125